INTERNATIONAL JOURNAL FOR NUMERICAL METHODS IN FLUIDS
Int. J. Numer. Meth. Fluids 2010; **63**:533–547
Published online 8 June 2009 in Wiley InterScience (www.interscience.wiley.com). DOI: 10.1002/fld.2084

Stability of flow past a cylinder: Energy budget of eigenmodes

Sanjay Mittal*, †

Department of Aerospace Engineering, Indian Institute of Technology Kanpur, UP 208 016, India

SUMMARY

Global linear stability analysis of the flow past a circular cylinder at the onset of primary wake instability is carried out. The real and imaginary parts of the most unstable eigenmode, responsible for vortex shedding, are very similar but associated with a spatial shift in the vortex structures. This shift results in the convection of vortices that are observed in the unsteady flow, which is actually a consequence of global absolute instability. The kinetic energy density, associated with the most unstable eigenmode, is studied. At the onset of the instability the energy density of the disturbance field is found to be stronger in the far wake compared with the near wake. With increase in Re the region where the disturbance is strong moves upstream closer to the cylinder. However, the maximum value of the kinetic energy density of the disturbance lies outside the recirculation zone even for Re upto 100. A linearized mechanical energy equation for the time evolution of the kinetic energy density of the disturbance is utilized to examine the energy budget of the most unstable eigenmode at various Re. It is found that the most significant contribution to the growth rate of the disturbance arises from the transfer of the energy due to the strain rate of the base flow to the perturbation. The stabilizing effect of the viscous dissipation increases with increase in Re, but saturates for Re beyond $\sim$70.

Received 30 April 2008; Revised 1 April 2009; Accepted 9 April 2009

KEY WORDS: global instability; flow past cylinder; energy budget; linear stability analysis; stabilized finite element method; absolute instability

1. INTRODUCTION

The flow past a cylinder looses stability at $Re \sim 47$ [1–3]. The Reynolds number is defined as $Re = \rho U D/\mu$, where ρ, U, D and μ are the fluid density, free-stream speed, diameter of the cylinder and coefficient of viscosity of the fluid, respectively. Various researchers in the past have utilized global linear stability analysis (LSA) to study the primary instability of the wake [3–7]. It is well known that this instability of the flow, which sets in via a Hopf bifurcation, is an example

*Correspondence to: Sanjay Mittal, Department of Aerospace Engineering, Indian Institute of Technology Kanpur, UP 208 016, India.
†E-mail: smittal@iitk.ac.in

Contract/grant sponsor: Department of Science and Technology

of global absolute instability and is responsible for the von Karman vortex shedding. In this case there are stationary perturbations (unstable eigenmodes) that grow with time. This is in contrast to the global convective instability, in which case there exists a traveling perturbation that grows with time.

The notion of absolute/convective instability was originally developed for parallel flows. In a parallel flow an absolute instability can be viewed as a convective instability by an appropriate change of the frame of reference and vice versa. Thus, the notion of absolute/convective instability acquires physical significance when the underlying Galilean invariance is broken. For nonparallel flows, the notion of absolute/convective instability can be extended via a local analysis, which is based on parallel flow theory. A detailed discussion of the absolute/convective instability concepts from the point of view of local analysis of hydrodynamic flows is presented in the review paper by Huerre and Monkewitz [8]. Recently, Mittal and Kumar [7] proposed a method to carry out a global convective instability analysis for a nonparallel flow [7].

In view of the above discussion, we describe two approaches to the LSA of nonparallel flows: local analysis of the assumed parallel flow and global nonparallel flow theory. In a local analysis, one assumes the flow profile at a station of interest in the flow field to be parallel and determines its stability characteristics via Rayleigh or Orr–Sommerfeld equation [9]. The resulting instability, if it exists, may be absolute or convective in nature. A local instability, however, does not necessarily result in a global instability. Linear stability theory can also be applied to the entire nonparallel flow [7].

In this paper the global LSA of the flow past a cylinder is carried out. The focus is on the global absolute instability. In the remainder of this paper the absolute/convective instability should be interpreted in the global sense, unless stated otherwise. An energy equation for the evolution of the kinetic energy density of the disturbance field is developed from the linearized disturbance equation (LDE). Since the most unstable eigenmodes are complex in nature the energy equation is written for a general complex disturbance. For this purpose, the energy equation presented by Drazin [10] is generalized for a complex disturbance. The equation is further worked out for the case when the disturbance field corresponds to the most unstable eigenmode from the LSA of the flow. By integrating the equation for the kinetic energy density over the domain, a relation for the growth rate of the disturbance is derived, which shows the contributions from the various mechanisms. These mechanisms are: the convection of the disturbance by the base flow, energy transferred from the strain rate field of the base flow to the perturbation, work done by the perturbation pressure gradient and viscous dissipation of energy.

Some of the questions that we attempt to address in this paper are as follows. With respect to the recirculation region, where does the maximum kinetic energy density occur for the most unstable eigenmode? What is the relative role of the various mechanisms that lead to the instability? It is well known that the vortex shedding arises due to an absolute instability. From the point of view of local analysis, it is well established that a global mode emerges out of a much larger region of convective instability. Therefore, the vortices are seen to convect downstream following the onset of primary instability of the wake. However, from the point of view of global analysis, it is not clear as to why a global mode, that is absolutely unstable, leads to the convection of vortices during vortex shedding?

The incompressible flow equations, in the velocity pressure form, are solved via a stabilized finite element method. The stabilized formulation is based on the streamline-upwind/Petrov–Galerkin (SUPG) and pressure-stabilizing/Petrov–Galerkin (PSPG) stabilization techniques [11]. Several element-level integrals are added to the Galerkin formulation to stabilize the computations

DOI: 10.1002/fld

against spurious numerical oscillations. The basic Galerkin formulation is unstable for convection-dominated flows and does not allow one to use equal-order interpolation velocity–pressure elements. The formulation for the LSA with the stabilized finite element method, being used here, was proposed in one of our earlier works [12]. The LSA involves the solution to an eigenvalue problem. A subspace iteration procedure [5] in conjunction with shift-invert transformation is utilized.

2. THE GOVERNING EQUATIONS

2.1. The incompressible flow equations

The equations governing the flow of an incompressible fluid are:

$$\rho\left(\frac{\partial \mathbf{u}}{\partial t}+\mathbf{u}\cdot\nabla\mathbf{u}-\mathbf{f}\right)-\nabla\cdot\boldsymbol{\sigma}=\mathbf{0} \quad \text{on } \Omega\times(0,T) \tag{1}$$

$$\nabla\cdot\mathbf{u}=0 \quad \text{on } \Omega\times(0,T) \tag{2}$$

Here, ρ, $\mathbf{u}$, $\mathbf{f}$ and $\boldsymbol{\sigma}$ are the density, velocity, body force and the stress tensor, respectively. For a Newtonian fluid the stress tensor is given as $\boldsymbol{\sigma}=-p\mathbf{I}+2\mu\boldsymbol{\varepsilon}(\mathbf{u})$, where $\boldsymbol{\varepsilon}$ is the strain rate given as $\boldsymbol{\varepsilon}(\mathbf{u})=\frac{1}{2}((\nabla\mathbf{u})+(\nabla\mathbf{u})^{\mathrm{T}})$. Here, p and μ are the pressure and coefficient of the dynamic viscosity, respectively. These equations are accompanied with appropriate boundary conditions on the velocity and stress and an initial condition on the velocity.

2.2. Global LSA

We decompose the unsteady flow, ($\mathbf{u}$, p) as a combination of the steady part and disturbance: $\mathbf{u}=\mathbf{U}+\mathbf{u}'$ and $p=P+p'$. Here, ($\mathbf{U}$, P) represent the steady-state solution obtained by solving Equations (1) and (2) without the unsteady terms. $\mathbf{u}'$ and p' are the perturbation fields of the velocity and pressure, respectively. Substituting for this decomposition in Equations (1)–(2) and subtracting from them, the equations for steady flow, one obtains the following equations for the disturbance fields:

$$\rho\left(\frac{\partial \mathbf{u}'}{\partial t}+\mathbf{u}'\cdot\nabla\mathbf{U}+\mathbf{U}\cdot\nabla\mathbf{u}'+\mathbf{u}'\cdot\nabla\mathbf{u}'\right)-\nabla\cdot\boldsymbol{\sigma}'=\mathbf{0} \tag{3}$$

$$\nabla\cdot\mathbf{u}'=0 \tag{4}$$

In the equation above $\boldsymbol{\sigma}'$ represents the stress tensor due to the perturbed solution ($\mathbf{u}'$, p'). We further assume that the disturbances are small and drop the nonlinear term. This leads to the LDE of the form:

$$\rho\left(\frac{\partial \mathbf{u}'}{\partial t}+\mathbf{u}'\cdot\nabla\mathbf{U}+\mathbf{U}\cdot\nabla\mathbf{u}'\right)-\nabla\cdot\boldsymbol{\sigma}'=\mathbf{0} \tag{5}$$

$$\nabla\cdot\mathbf{u}'=0 \tag{6}$$

For conducting the global LSA of the flow ($\mathbf{U}$, P) we assume the disturbance field of the following form:

$$\mathbf{u}'(\mathbf{x},t)=\hat{\mathbf{u}}(\mathbf{x})\mathrm{e}^{\lambda t}, \quad p'(\mathbf{x},t)=\hat{p}(\mathbf{x})\mathrm{e}^{\lambda t} \tag{7}$$

DOI: 10.1002/fld

This allows us to conduct a global, LSA of a general, nonparallel but steady flow. Substituting this form of the disturbance in Equations (5)–(6) we get:

$$\rho(\lambda\hat{\mathbf{u}}+\hat{\mathbf{u}}\cdot\nabla\mathbf{U}+\mathbf{U}\cdot\nabla\hat{\mathbf{u}})-\nabla\cdot\hat{\boldsymbol{\sigma}}=\mathbf{0} \tag{8}$$

$$\nabla\cdot\hat{\mathbf{u}}=0 \tag{9}$$

Here, λ is the eigenvalue of the fluid system and governs its stability. In general, $\lambda=\lambda_\mathrm{r}+\mathrm{i}\lambda_\mathrm{i}$, where λ_r and λ_i are the real and imaginary parts, respectively. Similarly, the eigenmode $\hat{\mathbf{u}}(\mathbf{x})$ is $\hat{\mathbf{u}}_\mathrm{r}(\mathbf{x})+\mathrm{i}\hat{\mathbf{u}}_\mathrm{i}(\mathbf{x})$, where $\hat{\mathbf{u}}_\mathrm{r}(\mathbf{x})$ and $\hat{\mathbf{u}}_\mathrm{i}(\mathbf{x})$ are the real and imaginary parts, respectively. The steady-state solution $(\mathbf{U}, P)$ is associated with an unstable mode if the rightmost eigenvalue has a positive real part. The boundary conditions for $(\hat{\mathbf{u}},\ \hat{p})$ are the homogeneous versions of the ones for $(\mathbf{U}, P)$.

2.3. The linearized mechanical energy equation for the disturbance field

Note that, in general, the eigenmodes for the velocity and pressure fields are complex. This leads to a complex field for the velocity and pressure perturbations: $(\mathbf{u}'(\mathbf{x},t), p'(\mathbf{x},t))$. Let $(\mathbf{u}', p')$ and $(\overline{\mathbf{u}'}, \overline{p'})$ be one such conjugate pair. These fields, independent of each other, satisfy the LDE given by Equations (5)–(6). We define the specific kinetic energy of the disturbance $e'(\mathbf{x},t)$ as:

$$e'(\mathbf{x},t)=\tfrac{1}{2}\mathbf{u}'(\mathbf{x},t)\cdot\overline{\mathbf{u}'}(\mathbf{x},t) \tag{10}$$

We take the dot product of Equation (5) with $\overline{\mathbf{u}'}$ and add it to the dot product of $\mathbf{u}'$ with Equation (5) written for the fields $(\overline{\mathbf{u}'}, \overline{p'})$. This leads to the equation for the evolution of e' and is given as:

$$\rho\frac{\partial e'}{\partial t}=-\rho\mathbf{U}\cdot\nabla e'-\rho\mathbf{u}'\overline{\mathbf{u}'}:\boldsymbol{\varepsilon}(\mathbf{U})-(\mathbf{u}'\cdot\nabla\overline{p'}+\overline{\mathbf{u}'}\cdot\nabla p')-\mu(\nabla\mathbf{u}':\nabla\overline{\mathbf{u}'}-\Delta e') \tag{11}$$

In this equation the term on the left-hand side represents the time rate of change of the kinetic energy density of the disturbance. The first term on the RHS, $-\rho\mathbf{U}\cdot\nabla e'$, represents the convection, by the base flow, of the kinetic energy of the disturbance. The second term on the RHS, $-\rho\mathbf{u}'\overline{\mathbf{u}'}:\boldsymbol{\varepsilon}(\mathbf{U})$, is the energy extracted by the disturbance from the base flow. The third term, $-(\mathbf{u}'\cdot\nabla\overline{p'}+\overline{\mathbf{u}'}\cdot\nabla p')$, is the rate of work done by the pressure disturbance, whereas the last term corresponds to the work done by the viscous forces.

Recall that the disturbance field can be written in terms of eigenmodes as given by Equation (7). Therefore, the specific kinetic energy of the disturbance field can be expressed as

$$e'(\mathbf{x},t)=\hat{e}(\mathbf{x})\mathrm{e}^{2\lambda_\mathrm{r}t} \tag{12}$$

where $\hat{e}(\mathbf{x})=\frac{1}{2}\hat{\mathbf{u}}(\mathbf{x})\cdot\overline{\hat{\mathbf{u}}}(\mathbf{x})$. From Equation (12) we note that

$$\frac{\partial e'}{\partial t}=2\lambda_\mathrm{r}e' \tag{13}$$

We recall two observations that can be made regarding the local time evolution of the specific kinetic energy from this equation. First, it shows that the energy of an unstable global mode grows everywhere with twice the growth rate of the disturbance. Second, the time rate of kinetic energy of a global mode has the same spatial structure as that of the energy distribution itself. Substituting

DOI: 10.1002/fld

this decomposition in the energy equation, Equation (11), leads to

$$2\lambda_r\hat{e} = -\mathbf{U}\cdot\nabla\hat{e} - \hat{\mathbf{u}}\overline{\hat{\mathbf{u}}}:\boldsymbol{\varepsilon}(\mathbf{U}) - \tfrac{1}{\rho}(\hat{\mathbf{u}}\cdot\nabla\overline{\hat{p}} + \overline{\hat{\mathbf{u}}}\cdot\nabla\hat{p}) + \nu(\Delta\hat{e} - \nabla\hat{\mathbf{u}}:\nabla\overline{\hat{\mathbf{u}}}) \tag{14}$$

For future reference, we rewrite this equation as

$$\frac{\partial e'}{\partial t} = \left(\frac{\partial e'}{\partial t}\right)_{\text{convection}} + \left(\frac{\partial e'}{\partial t}\right)_{\text{transfer}} + \left(\frac{\partial e'}{\partial t}\right)_{\text{pressure}} + \left(\frac{\partial e'}{\partial t}\right)_{\text{viscous}} \tag{15}$$

where $(\partial e'/\partial t)_{\text{convection}} = -\mathbf{U}\cdot\nabla e'$, $(\partial e'/\partial t)_{\text{transfer}} = -\mathbf{u}'\overline{\mathbf{u}'}:\boldsymbol{\varepsilon}(\mathbf{U})$, $(\partial e'/\partial t)_{\text{pressure}} = -1/\rho(\mathbf{u}'\cdot\nabla\overline{p'} + \overline{\mathbf{u}'}\cdot\nabla p')$ and $(\partial e'/\partial t)_{\text{viscous}} = -\nu(\nabla\mathbf{u}':\nabla\overline{\mathbf{u}'} - \Delta e')$ represent the contributions to the time rate of change of kinetic energy density of a disturbance field from various mechanisms. Next, we integrate the energy equation over the domain of the flow, Ω. We assume that Ω is fixed for all t and define $\hat{E} = \int_\Omega \hat{e}\,\mathrm{d}\Omega$. For an unbounded flow the boundary condition at the outflow corresponds to setting the flow variables to their free-stream values. However, for a finite domain this may lead to large inaccuracies. In the present work, the stress vector at the outflow boundary is assigned as zero value. In view of this we rearrange Equation (14) and integrate it over the domain. This leads to:

$$\lambda_r = -\frac{1}{2\hat{E}}\int_\Omega \mathbf{U}\cdot\nabla\hat{e}\,\mathrm{d}\Omega - \frac{1}{2\hat{E}}\int_\Omega \hat{\mathbf{u}}\overline{\hat{\mathbf{u}}}:\boldsymbol{\varepsilon}(\mathbf{U})\,\mathrm{d}\Omega + \frac{\mu}{\rho\hat{E}}\int_\Omega (\boldsymbol{\varepsilon}(\hat{\mathbf{u}}):\boldsymbol{\varepsilon}(\overline{\hat{\mathbf{u}}}))\,\mathrm{d}\Omega \tag{16}$$

For future reference, we rewrite this equation as

$$\lambda_r = (\lambda_r)_{\text{convection}} + (\lambda_r)_{\text{transfer}} + (\lambda_r)_{\text{viscous}} \tag{17}$$

where

$$(\lambda_r)_{\text{convection}} = -\frac{1}{2\hat{E}}\int_\Omega \mathbf{U}\cdot\nabla\hat{e}\,\mathrm{d}\Omega, \quad (\lambda_r)_{\text{transfer}} = -\frac{1}{2\hat{E}}\int_\Omega \hat{\mathbf{u}}\overline{\hat{\mathbf{u}}}:\boldsymbol{\varepsilon}(\mathbf{U})\,\mathrm{d}\Omega$$

and

$$(\lambda_r)_{\text{viscous}} = \frac{\mu}{\rho\hat{E}}\int_\Omega (\boldsymbol{\varepsilon}(\hat{\mathbf{u}}):\boldsymbol{\varepsilon}(\overline{\hat{\mathbf{u}}}))\,\mathrm{d}\Omega$$

are the contributions to the growth rate from the various mechanisms. We note that the pressure does not contribute to the overall growth rate of the disturbance. In addition, it can be shown that $(\lambda_r)_{\text{convection}}$ results in a nonzero value only if $\hat{e}$ does not vanish at the outflow boundary. Equation (17) can also be utilized to recover the value of growth rate, λ_r, from the eigenmodes $(\hat{\mathbf{u}},\ \hat{p})$.

3. THE FINITE ELEMENT FORMULATION

3.1. The incompressible flow equations

Consider a finite element discretization of the domain, Ω, into subdomains Ω^e, $e = 1, 2, \ldots, n_{\text{el}}$, where n_{el} is the number of elements. Based on this discretization let $\mathscr{S}^h_{\mathbf{u}}$ and $\mathscr{S}^h_p$ be the finite element trial function spaces for velocity and pressure, respectively, and $\mathscr{V}^h_{\mathbf{u}}$ and $\mathscr{V}^h_p$ be the weighting function spaces. The stabilized finite element formulation of Equations (1)–(2) is written

DOI: 10.1002/fld

as follows: find $\mathbf{u}^h \in \mathscr{S}^h_{\mathbf{u}}$ and $p^h \in \mathscr{S}^h_p$ such that $\forall \mathbf{w}^h \in \mathscr{V}^h_{\mathbf{u}}$, $q^h \in \mathscr{V}^h_p$

$$\int_\Omega \mathbf{w}^h \cdot \rho \left(\frac{\partial \mathbf{u}^h}{\partial t} + \mathbf{u}^h \cdot \nabla \mathbf{u}^h - \mathbf{f} \right) \mathrm{d}\Omega + \int_\Omega \boldsymbol{\varepsilon}(\mathbf{w}^h) : \boldsymbol{\sigma}(p^h, \mathbf{u}^h) \, \mathrm{d}\Omega$$
$$+ \int_\Omega q^h \nabla \cdot \mathbf{u}^h \, \mathrm{d}\Omega + \sum_{e=1}^{n_{\mathrm{el}}} \int_{\Omega^e} \frac{1}{\rho} (\tau_{\mathrm{SUPG}} \rho \mathbf{u}^h \cdot \nabla \mathbf{w}^h + \tau_{\mathrm{PSPG}} \nabla q^h)$$
$$\cdot \left[\rho \left(\frac{\partial \mathbf{u}^h}{\partial t} + \mathbf{u}^h \cdot \nabla \mathbf{u}^h - \mathbf{f} \right) - \nabla \cdot \boldsymbol{\sigma}(p^h, \mathbf{u}^h) \right] \mathrm{d}\Omega^e$$
$$+ \sum_{e=1}^{n_{\mathrm{el}}} \int_{\Omega^e} \tau_{\mathrm{LSIC}} \nabla \cdot \mathbf{w}^h \rho \nabla \cdot \mathbf{u}^h \, \mathrm{d}\Omega^e = \int_{\Gamma_h} \mathbf{w}^h \cdot \mathbf{h}^h \, \mathrm{d}\Gamma \tag{18}$$

Here, Γ_g and Γ_h are complementary subsets of the boundary Γ on which Dirichlet and Neumann-type boundary conditions are assigned as follows:

$$\mathbf{u} = \mathbf{g} \quad \text{on } \Gamma_g, \quad \mathsf{n} \cdot \boldsymbol{\sigma} = \mathbf{h} \quad \text{on } \Gamma_h \tag{19}$$

where n is the unit normal vector to Γ_h. In the variational formulation given by Equation (18), the first three terms and the right-hand side constitute the Galerkin formulation of the problem. It is well known that the Galerkin formulation is unstable with respect to the advection operator as the cell Reynolds number (based on the local flow velocity and mesh size) becomes larger. Also, not all combinations of the velocity and pressure interpolations are admissible in the Galerkin formulation. Elements that do not satisfy the Babuska–Brezzi condition lead to oscillatory solutions and sometimes to no solution at all. To give stability to the basic formulation, a series of element-level integrals are added. The first series of element-level integrals are the SUPG and PSPG stabilization terms added to the variational formulations [11]. The SUPG formulation for convection-dominated flows was introduced by Hughes and Brooks [13] and Brooks and Hughes [14]. The Petrov–Galerkin term for Stokes flows, to admit the use of equal-order interpolations for velocity and pressure without producing oscillations in the pressure field, was proposed by Hughes *et al.* [15]. Tezduyar *et al.* [11] proposed a formulation using the SUPG and PSPG stabilizations for finite Reynolds number flows. The second series of element-level integrals are the stabilization terms based on the least squares of the divergence-free condition on the velocity field. The definitions for τ_{PSPG} and τ_{SUPG} are given by the following relations based on their values for the advection and diffusion limits.

$$\tau_{\mathrm{SUPG}} = \tau_{\mathrm{PSPG}} = \left(\frac{1}{\tau^2_{\mathrm{ADV}}} + \frac{1}{\tau^2_{\mathrm{DIF}}} \right)^{-1/2} \tag{20}$$

where

$$\tau_{\mathrm{ADV}} = \frac{h^e}{2\|\mathbf{u}^h\|}, \quad \tau_{\mathrm{DIF}} = \frac{(h^e)^2}{12\nu} \tag{21}$$

Here, h^e is the element length and various definitions have been used by researchers in the past. Mittal [16] conducted a systematic numerical study to investigate the effect of high aspect ratio elements on the performance of the finite element formulation for three commonly used definitions of h^e. In this work we use the definition based on the minimum edge length of an element. The

DOI: 10.1002/fld

coefficient τ_{LSIC} is defined as

$$\tau_{\mathrm{LSIC}} = \left(\frac{1}{\delta_{\mathrm{ADV}}^2} + \frac{1}{\delta_{\mathrm{DIF}}^2} \right)^{-1/2} \tag{22}$$

where

$$\delta_{\mathrm{ADV}} = \frac{h^e \|\mathbf{u}^h\|}{2}, \quad \delta_{\mathrm{DIF}} = \frac{(h^e)^2 (\|\mathbf{u}^h\|)^2}{12\nu} \tag{23}$$

The implicit method used in the present work allows us to seek steady-state solutions by simply dropping the unsteady terms in the governing equations.

3.2. The linear stability equations

Let $\hat{\mathscr{S}}_{\mathbf{u}}^h$ and $\hat{\mathscr{S}}_p^h$ be the finite element trial function spaces and $\hat{\mathscr{V}}_{\mathbf{u}}^h$ and $\hat{\mathscr{V}}_p^h$ the weighting function spaces for the perturbations in the velocity and pressure fields, respectively. The finite element formulation for the perturbation equations, (8) and (9), is given as: find $\hat{\mathbf{u}}^h \in \hat{\mathscr{S}}_{\mathbf{u}}^h$ and $\hat{p}^h \in \hat{\mathscr{S}}_p^h$ such that $\forall \hat{\mathbf{w}}^h \in \hat{\mathscr{V}}_{\mathbf{u}}^h$ and $\hat{q}^h \in \hat{\mathscr{V}}_p^h$

$$\begin{aligned}
&\int_\Omega \hat{\mathbf{w}}^h \cdot \rho(\lambda \hat{\mathbf{u}}^h + \mathbf{U}^h \cdot \nabla \hat{\mathbf{u}}^h + \hat{\mathbf{u}}^h \cdot \nabla \mathbf{U}^h)\, \mathrm{d}\Omega + \int_\Omega \boldsymbol{\varepsilon}(\hat{\mathbf{w}}^h) : \boldsymbol{\sigma}(\hat{p}^h, \hat{\mathbf{u}}^h)\, \mathrm{d}\Omega \\
&+ \int_\Omega \hat{q}^h \nabla \cdot \hat{\mathbf{u}}^h \, \mathrm{d}\Omega + \sum_{e=1}^{n_{\mathrm{el}}} \int_{\Omega^e} \frac{1}{\rho} (\tau_{\mathrm{SUPG}} \rho \mathbf{U}^h \cdot \nabla \hat{\mathbf{w}}^h + \tau_{\mathrm{PSPG}} \nabla \hat{q}^h) \\
&\cdot [\rho(\lambda \hat{\mathbf{u}}^h + \mathbf{U}^h \cdot \nabla \hat{\mathbf{u}}^h + \hat{\mathbf{u}}^h \cdot \nabla \mathbf{U}^h) - \nabla \cdot \boldsymbol{\sigma}(\hat{p}^h, \hat{\mathbf{u}}^h)]\, \mathrm{d}\Omega^e \\
&+ \sum_{e=1}^{n_{\mathrm{el}}} \int_{\Omega^e} \tau_{\mathrm{LSIC}} \nabla \cdot \hat{\mathbf{w}}^h \rho \nabla \cdot \hat{\mathbf{u}}^h \, \mathrm{d}\Omega^e = 0
\end{aligned} \tag{24}$$

The stabilization coefficients for the LSA are given by the same definition as defined in Equations (20)–(23) except that they are based on the steady-state velocity field, $\mathbf{U}^h$. Equation (24) leads to a generalized eigenvalue problem of the form $\mathbf{A}X - \lambda \mathbf{B}X = 0$, where $\mathbf{A}$ and $\mathbf{B}$ are nonsymmetric matrices. In this study we use the shift-invert transformation in conjunction with the subspace iteration method [17] to track the eigenvalue with the largest real part.

4. PROBLEM SETUP

The cylinder resides in a computational domain whose outer boundary is a rectangle. The radius of the cylinder is 1 unit; time is nondimensionalized using the free-stream speed and the radius of the cylinder. A schematic of the problem setup is shown in Figure 1. All the boundaries are located at a distance of $50D$ from the center of the cylinder, where D is the diameter of the cylinder. The finite element mesh, used in this work, consists of 40 432 quadrilateral elements and 40 920 nodes. The structure of the mesh is the same as the one used in our earlier studies (for example, [12]). The following boundary conditions are applied. Free-stream value is assigned to the velocity at

DOI: 10.1002/fld

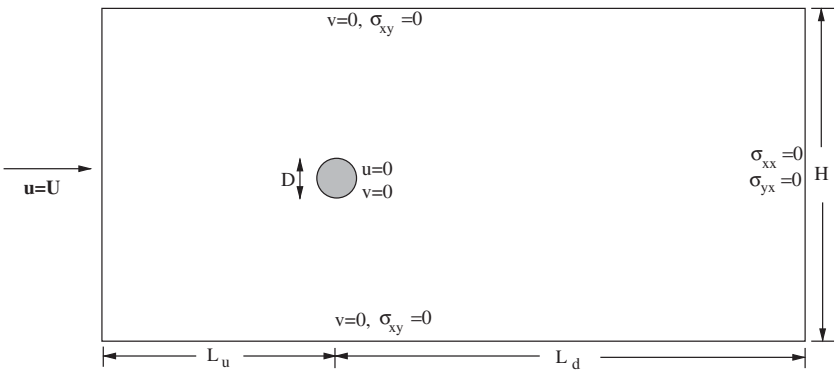

Figure 1. Flow past a circular cylinder: schematic of the computational domain and the boundary conditions.

the upstream boundary. At the downstream boundary, a Neumann-type boundary condition for the velocity is specified which corresponds to zero stress vector. On the upper and lower boundaries a 'slip-wall' boundary condition is employed, i.e. the component of velocity normal to and the component of stress vector along these boundaries are prescribed a zero value. For the LSA the boundary conditions are the homogeneous versions of the ones used for determining the steady-state solutions.

5. RESULTS

5.1. The steady flow

First, the steady flow is computed for various Re by dropping the time-dependent terms from Equations (1)–(2). Excellent agreement is observed with the results from other researchers. For example, at $Re=100$ the length of the bubble from the present computations is $6.65D$ and the drag coefficient is 1.0651. The values from Fornberg [18] are $6.6D$ and 1.072, respectively. Gajjar and Azzam [19] reported the values to be $6.64D$ and 1.079, respectively. The computations by Fornberg [18] and Gajjar and Azzam [19] have been carried out for one half of the cylinder.

5.2. Linear stability analysis

Once the steady-state solution is available, at each Re, the global stability analysis is carried out. Figure 2 shows the variation of the real part of the eigenvalue with Re. The flow becomes absolutely unstable at $Re\sim47$. The St at the onset of vortex shedding is found to be 0.1168. The real and imaginary parts of the most unstable eigenmode for $Re=42,\ 70$ and 100 are shown in Figure 3. The eigenfunctions are normalized such that the Euclidean norm of the vector formed by the values of velocity and pressure, of the real as well as imaginary components at all nodes, are unity. The dark shades of gray denote the negative values, whereas the lighter shades represent positive values. The y component of velocity and the vorticity fields of the most unstable eigenmode is symmetric about the wake centerline. However, the x component of velocity and the pressure fields of the eigenmode is skew-symmetric. The symmetry properties of the steady flow are exactly the opposite. For example, the vorticity field of the steady flow is skew-symmetric about the

DOI: 10.1002/fld

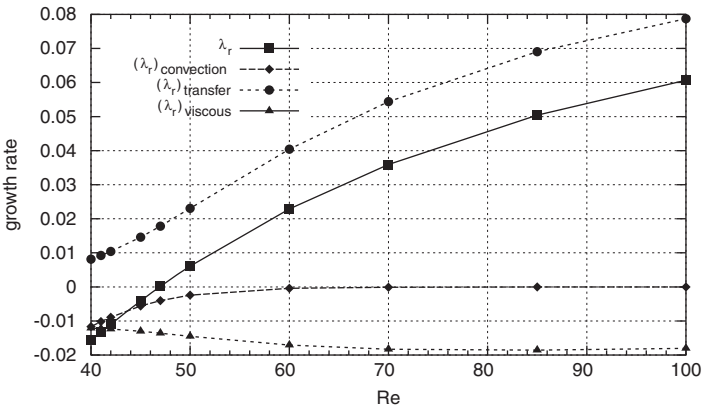

Figure 2. Linear stability analysis for flow past a circular cylinder: real part of the rightmost eigenvalue for various Re (in solid line). The contributions to the growth rate from convection, energy transfer and viscous mechanisms are also shown.

wake centerline. The superposition of the steady and disturbance field, therefore, does not exhibit any symmetry about the centerline. In that sense, the instability being considered is a symmetry breaking bifurcation [20].

From Figure 3 it can be observed that the real and imaginary parts of the eigenmodes are structurally very similar. However, the vortex structures seem to be separated by a spatial phase. This phase separation or the spatial stagger in the vortex structures coupled with the imaginary part of the eigenvalue is responsible for the convection of vortices in the primary instability of the wake. Recall that the primary instability of the wake is a consequence of an absolute instability. The convection of vortices in a flow driven by an absolute instability is observed in several other situations and may be caused by the same phenomenon observed here. It can also be observed from Figure 3 that as the Re increases the disturbance field tends to become stronger and closer to the cylinder and the region of maximum relative disturbance shifts upstream. For example, compared with $Re=70$, the disturbance field in the far downstream region at $Re=100$ is quite weak.

5.3. Kinetic energy density of the disturbance field

The real and imaginary parts of the most unstable eigenmode are utilized to compute the kinetic energy density of the disturbance field via Equation (10). The energy fields for various Re are shown in Figure 4. The recirculation bubble for the steady flow at each Re is also shown in the same figure. The results are in good agreement with the energy distribution shown by Gianetti and Luchini [21] for $Re=50$. These figures show the spatial structure of the disturbance field. The observations made from the eigenmode regarding the strength of the disturbance field are much clearer from these pictures. At $Re=42$ the disturbance field is strong in the far wake and very weak in the near wake. With increase in Re the region in which the disturbance field is strong moves closer to the cylinder. At $Re=100$, the energy of the disturbance is large in the near wake and very small in the far wake. Figure 4 shows the x-location of the point where the energy of the disturbance field is maximum for various Re. The variation of the length of recirculation region of the steady flow with Re is also shown. While the bubble length increases linearly with Re, the

DOI: 10.1002/fld

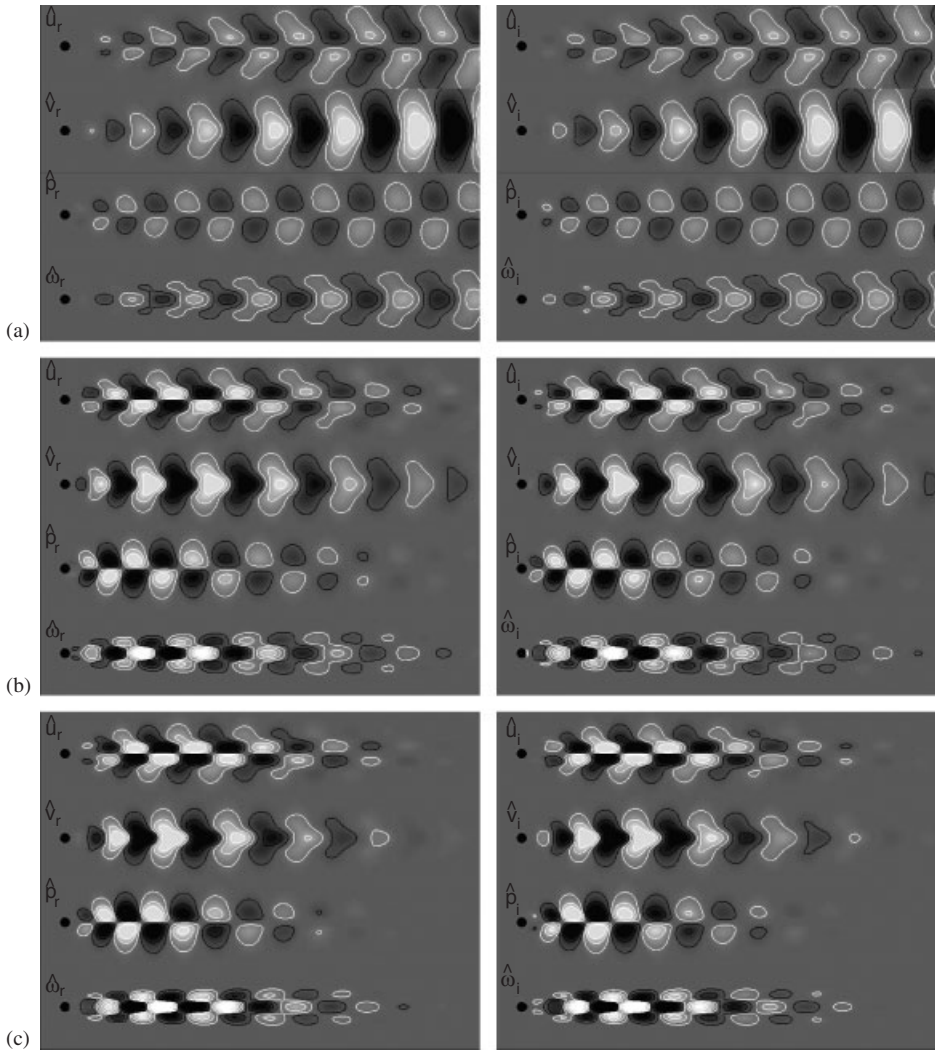

Figure 3. Linear stability analysis for flow past a circular cylinder: real (left) and imaginary (right) parts of the most unstable eigenmode for: (a) $Re=42$; (b) $Re=70$; and (c) $Re=100$. The various panels show the velocity components, pressure and vorticity fields. Darker shades of gray represent negative values, whereas the lighter shades show positive values.

location of maximum kinetic energy density moves closer to the cylinder with increase in Re. It decreases quite rapidly with Re for low values of Re and then appears to settle at the value that remains constant with Re. Interestingly, in all the cases shown the maximum kinetic energy density is achieved outside the recirculation region. Gianetti and Luchini [21] also found that the location of the maximum kinetic energy moves downstream with decrease in Re. A similar prediction was made by Goujon-Durand *et al.* [22] via a nonlinear analysis.

DOI: 10.1002/fld

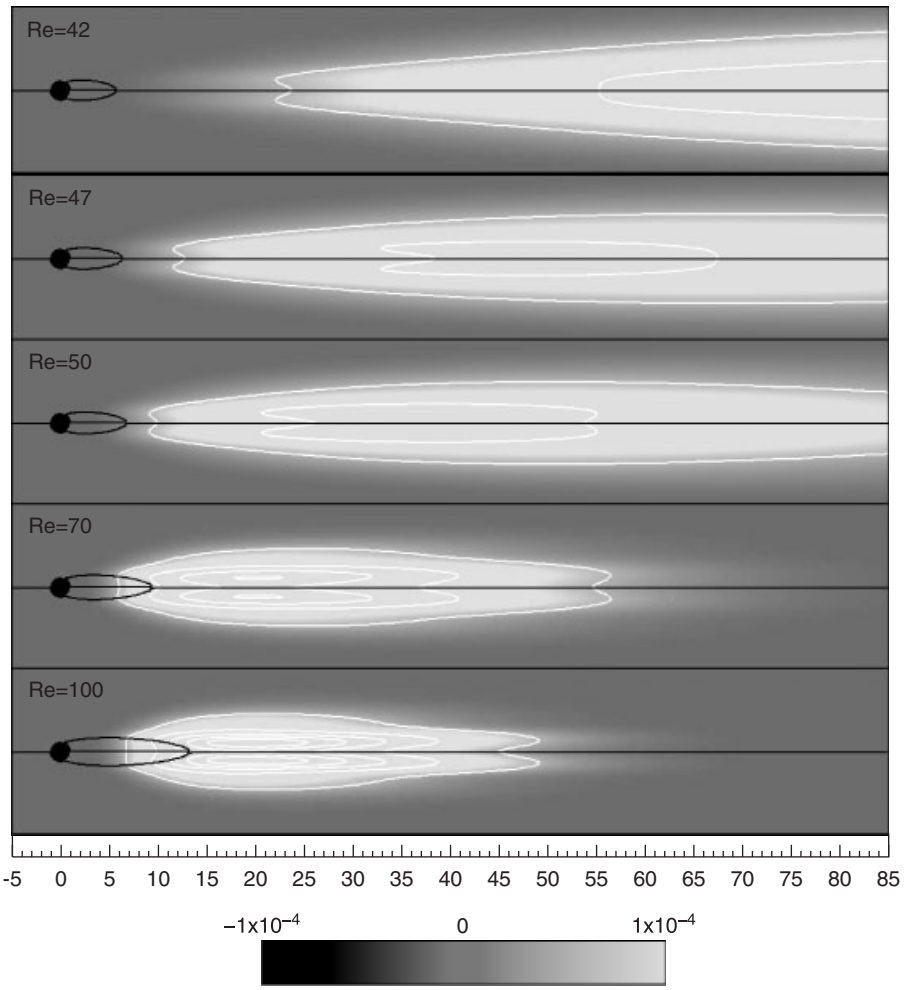

Figure 4. Linear stability analysis for flow past a circular cylinder: kinetic energy density field associated with the most unstable eigenmode for various Re. Also shown in the black line is the stagnation streamline for the steady flow at each Re. Darker shades of gray represent negative values, whereas the lighter shades show positive values.

5.4. Contribution to growth rate from various mechanisms

Equations (16) and (17) can be utilized to determine the contribution to the growth rate of the most unstable eigenmode from various mechanisms. Figure 2 shows the result for this computation at various Re. As expected, $(\lambda_r)_{viscous}$ is negative for all Re reflecting the stabilizing effect of viscous terms. In fact, the stabilizing effect increases with Re, for $Re<70$, and then remains virtually constant for larger Re. The term due to the convection of the disturbance energy by the base flow has a mild stabilizing effect for $Re<60$, approximately. For larger Re, as the disturbance becomes weaker at the outflow boundary, its contribution becomes insignificant. $(\lambda_r)_{transfer}$ is the

DOI: 10.1002/fld

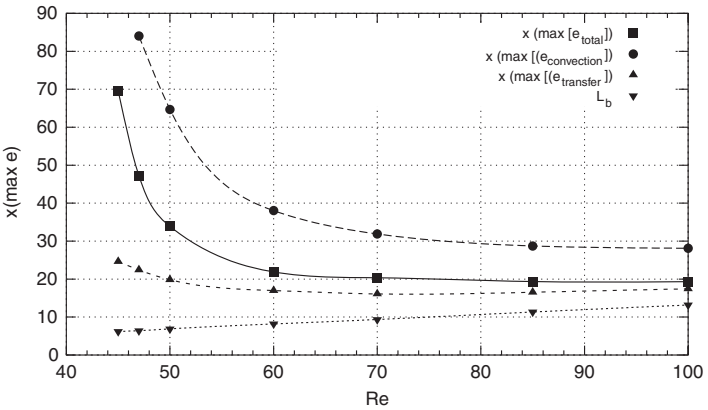

Figure 5. Linear stability analysis for flow past a circular cylinder: x-location of the point where the kinetic energy density of the most unstable disturbance field achieves maximum for various Re. Also shown is the variation of the bubble length with Re and the location of the maximum of the contribution, to the energy growth rate, from various mechanisms.

only contributor to the global instability of the flow and is positive for all the Re investigated. The destabilization related to the transfer of energy due to the strain rate of the base flow increases with increasing Re.

5.5. *Spatial distribution of the rate of increase of kinetic energy density*

Equation (13) shows that the local rate of increase of kinetic energy density for a global mode has the same spatial structure as the energy density distribution itself. We utilize Equation (15) to find the spatial distribution of the contribution of various mechanisms to the growth of kinetic energy density. Figure 6 shows the contributions from the transfer, convection, pressure and viscous-related mechanisms for $Re=50$ and 100. Dark shades of gray reflect a negative growth rate, whereas the lighter shades of gray denote a positive growth rate of local kinetic energy density. The mechanism related to the transfer of energy due to the strain rate of the base flow is the main contributor to the growth of kinetic energy density. With increase in Re, the location at which the maximum growth rate occurs, moves upstream. This can also be seen from Figure 5. While the global effect of the convection mechanism is stabilizing, it does have a local destabilizing effect in certain regions of the flow. Similarly, even though the pressure term has no contribution toward the global change in kinetic energy, there are regions in the flow where the local contributions are nontrivial. The viscous terms are responsible for the stabilizing effect everywhere in the flow domain.

6. CONCLUSION

Global LSA of the flow past a circular cylinder has been carried out. The flow undergoes a global absolute instability at $Re\sim47$ via a symmetry-breaking Hopf bifurcation. The steady flow and its most unstable eigenmode have complementary symmetry properties. For example, the vorticity field of the steady flow is skew-symmetric about the wake centerline while it is symmetric for the disturbance field. Consequently, the superposition of the steady flow and the most unstable

DOI: 10.1002/fld

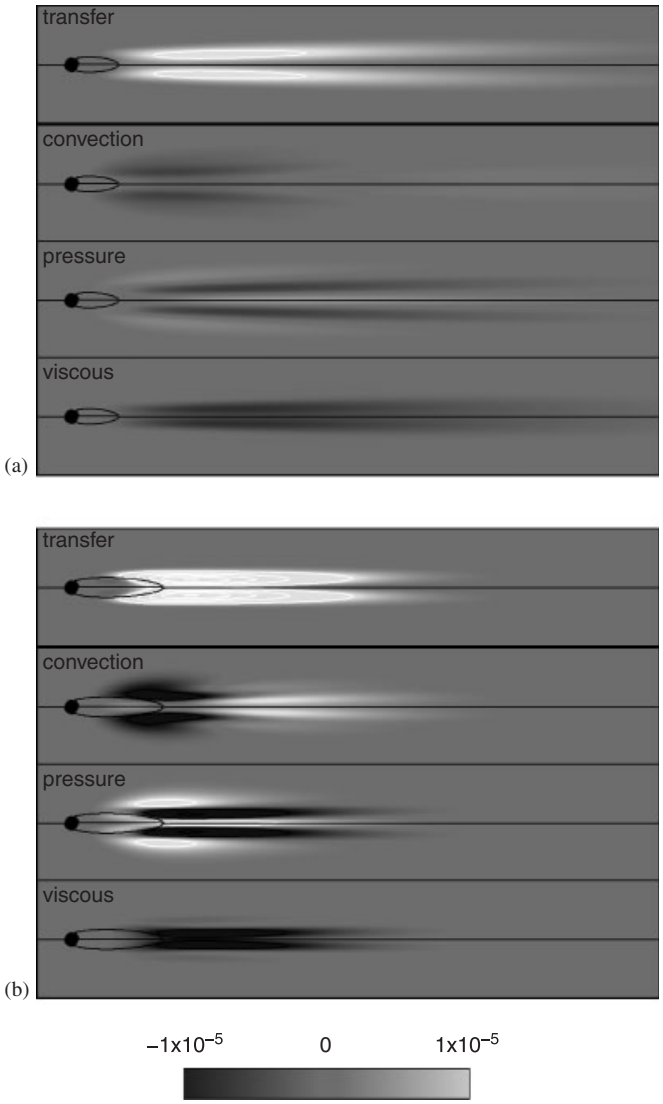

Figure 6. Linear stability analysis for flow past a circular cylinder: contributions to the local rate of increase of kinetic energy density of the disturbance from transfer, convection, pressure and viscous-related mechanisms (please see Equation (15)) for (a) $Re = 50$ and (b) $Re = 100$. Darker shades of gray represent negative values, whereas the lighter shades show positive values. Also shown is the stagnation streamline for the steady flow at each Re.

eigenmode leads to an asymmetric flow: the familiar von Karman vortex shedding. The real and imaginary parts of the unstable eigenmode, responsible for vortex shedding, look quite similar. However, there is a spatial stagger in the vortex structures of the two fields. This stagger is responsible for the convection of vortices that are observed in the unsteady flow, which is otherwise a consequence of an absolute instability.

DOI: 10.1002/fld

At the onset of instability, the kinetic energy density of the disturbance field is found to be stronger in the far wake and very weak in the near wake. With increase in Re the region where the disturbance is strong moves upstream, closer to the cylinder. It is found that the maximum value of the kinetic energy density of the disturbance lies outside the recirculation zone even for Re upto 100.

A linearized mechanical energy equation has been utilized to study the contribution of the various mechanisms toward the growth of the kinetic energy density of the disturbance field at the local as well as the global level. It is shown that the pressure does not play any role in the global kinetic energy evolution of the disturbance. The terms due to the convection of the disturbance by the base flow have a stabilizing effect for low Re. Their effect becomes insignificant for larger Re as the disturbance field becomes weak at the outflow boundary. As expected, the viscous terms have a stabilizing effect. The mechanism related to the transfer of energy due to the strain rate of the base flow is the one that is found to be responsible for the primary wake instability.

The spatial distribution of the local growth rate of the kinetic energy density of the most unstable disturbance is studied. Although the overall global effect of the convection of the disturbance by the base flow is stabilizing, it does contribute to instability locally in certain regions of the flow. Similarly, the pressure term is found to contribute to the growth and decay of the local kinetic energy density in some areas of the flow domain.

A new tool has been developed to study the energy budget of disturbance fields. It can be applied to other flows to increase the understanding of the mechanisms responsible for instabilities.

ACKNOWLEDGEMENTS

Partial support for this work from the Department of Science & Technology, India is gratefully acknowledged. The author also acknowledges the very useful discussions with Mr Bhaskar Kumar and his help in the preparation of the manuscript.

REFERENCES

1. Bénard H. Formation de centres de giration á l'arriére d'un obstacle en mouvement. *Comptes Rendus de l' Acadèmie des Sciences*, *Paris* 1908; **147**:839–842.
2. von Kármán T. Über den mechanismus des widerstandes, den ein bewegter körper in einer flüssigkeit erfährt. *Nachrichten der Akademie der Wissenschaften in Göttingen. II. Mathematisch-Physikalische Klasse* 1911; **12**: 509–519.
3. Jackson CP. A finite-element study of the onset of vortex shedding in flow past variously shaped bodies. *Journal of Fluid Mechanics* 1987; **182**:23–45.
4. Morzynski M, Thiele F. Numerical stability analysis of a flow about a cylinder. *Zeitschrift für Angewandte Mathematik und Mechanik* 1991; **71**:T424–T428.
5. Morzynski M, Afanasiev K, Thiele F. Solution of the eigenvalue problems resulting from global non-parallel flow stability analysis. *Computer Methods in Applied Mechanics and Engineering* 1999; **169**:161–176.
6. Ding Y, Kawahara M. Three dimensional linear stability analysis of incompressible viscous flows using the finite element method. *International Journal for Numerical Methods in Fluids* 1999; **31**:451–479.
7. Mittal S, Kumar B. A stabilized finite element method for global analysis of convective instabilities in nonparallel flows. *Physics of Fluids* 2007; **19**:88–105.
8. Huerre P, Monkewitz PA. Local and global instabilities in spatially developing flows. *Annual Review of Fluid Mechanics* 1990; **22**:473–537.
9. Drazin PG, Reid WH. *Hydrodynamic Stability*. Cambridge University Press: Cambridge, 1981.
10. Drazin PG. *Introduction to Hydrodynamic Stability*. Cambridge University Press: Cambridge, 2002.

DOI: 10.1002/fld

11. Tezduyar TE, Mittal S, Ray SE, Shih R. Incompressible flow computations with stabilized bilinear and linear equal-order-interpolation velocity–pressure elements. *Computer Methods in Applied Mechanics and Engineering* 1992; **95**:221–242.
12. Mittal S, Kumar B. Flow past a rotating cylinder. *Journal of Fluid Mechanics* 2003; **476**:303–334.
13. Hughes TJR, Brooks AN. A multi-dimensional upwind scheme with no crosswind diffusion. In *Finite Element Methods for Convection Dominated Flows*, Hughes TJR (ed.), AMD-vol. 34. ASME: New York, 1979; 19–35.
14. Brooks AN, Hughes TJR. Streamline upwind/Petrov–Galerkin formulations for convection dominated flows with particular emphasis on the incompressible Navier–Stokes equations. *Computer Methods in Applied Mechanics and Engineering* 1982; **32**:199–259.
15. Hughes TJR, Franca LP, Balestra M. A new finite element formulation for computational fluid dynamics: V. circumventing the Babuška–Brezzi condition: a stable Petrov–Galerkin formulation of the Stokes problem accommodating equal-order interpolations. *Computer Methods in Applied Mechanics and Engineering* 1986; **59**:85–99.
16. Mittal S. On the performance of high aspect-ratio elements for incompressible flows. *Computer Methods in Applied Mechanics and Engineering* 2000; **188**:269–287.
17. Stewart GW. Methods of simultaneous iteration for calculating eigenvectors of matrices. In *Topics in Numerical Analysis II*, Miller JHH (ed.). Academic Press: New York, 1975; 169–185.
18. Fornberg B. Steady incompressible flow past a row of circular cylinders. *Journal of Fluid Mechanics* 1991; **225**:655–671.
19. Gajjar JSB, Azzam N. Numerical solution of the Navier–Stokes equations for the flow in a cylinder cascade. *Journal of Fluid Mechanics* 2004; **520**:51–82.
20. Tang S, Aubry A. On the symmetry breaking instability leading to vortex shedding. *Physics of Fluids* 1997; **9**:2550–2561.
21. Giannetti F, Luchini P. Structural sensitivity of the first instability of the cylinder wake. *Journal of Fluid Mechanics* 2007; **581**:167–197.
22. Goujon-Durand S, Jenffer P, Wesfried JE. Downstream evolution of the Benardvon Karman instability. *Physical Review Letters* 1994; **50**:308–313.

DOI: 10.1002/fld